Electronic Supplementary Information

A reversible photochemical solid-state transformation in an interpenetrated 3D metal–organic framework with mechanical softness

Goutam Pahari[a], Biswajit Bhattacharya[a,b], C. Malla Reddy[b]* and Debajyoti Ghoshal[a]*

[a]Department of Chemistry, Jadavpur University, Jadavpur, Kolkata, 700 032, India

[b]Indian Institute of Science Education and Research (IISER) Kolkata, Mohanpur Campus, Mohanpur, 741 246, India.

Table of Contents

Experimental Section:

Materials. High purity Cadmium(II) nitrate tetrahydrate, 3,3-Dimethylglutaric acid (H_2-3,3-dmglu) and 1,2-bis(4-pyridyl)ethylene (bpe), were purchased from Sigma-Aldrich Chemical Co. Inc. and used as received. Disodium 3,3-Dimethylglutarate (Na_2-3,3- dmglu) was synthesized by the slow addition of solid Na_2CO_3 to aqueous solution of H_2-3,3-dmglu in a 1:1 ratio and was allowed to evaporate until dryness. All other chemicals including solvents were of AR grade and used as received.

Synthesis of {[Cd_2(bpe)$_2$(3,3-dmglu)$_2$]}$_n$ (1): Methanolic solution (20 mL) of 1,2-bis(4-pyridyl)ethylene (bpe) (1 mmol, 0.182 g) was mixed with an aqueous solution (20 mL) of disodium 3,3-dimethyl glutarate (Na_2-3,3- dmglu) (1 mmol, 0.204 g) to mix up well and in another beaker 20 ml aqueous solution of $Cd(NO_3)_2 \cdot 4H_2O$ (1 mmol, 0.308 g) was prepared. Then, 6 mL of this mixed ligand solution was slowly and carefully layered above 3 ml of metal solution using 5 mL buffer (1:1 MeOH and H_2O) in a glass tube. After ten days, linear shaped white colored single crystal of **1** was obtained at the wall of the tube with the yield of 60%; they were washed with methanol–water (1:1) mixture and dried. Anal. Calc. for $C_{38}H_{40}Cd_2N_4O_8$: C, 50.39; H, 4.45; N, 6.18. Found: C, 50.35; H, 4.40; N, 6.15. IR spectra (KBr, cm^{-1}): ν(CH–Ar),3100–2900; ν(C=C, Ar), 1530-1432; ν(CH–alkane), 1431-1354; ν(C=C), 1680–1560; ν(C–C), 1480; ν(C–H), 1393; ν(C–O),1250–1060. (Fig. S5) Details of crystallographic parameters are provided in Table S1, S2 and S3

{[Cd_2(rctt-tpcb)(3,3-dmglu)$_2$]}$_n$ (2): The single crystals of **2** were obtained by UV irradiation of single crystals of **1** for 4 h. Anal. Calc. for $C_{38}H_{40}Cd_2N_4O_8$: C, 50.39; H, 4.45; N, 6.18. Found: C, 50.38; H, 4.44; N, 6.18 %. IR spectra (KBr, cm^{-1}): ν(CH–Ar),3100–2900; ν(C=C, Ar), 1530-1432; ν(CH–alkane), 1431-1354; ν(C=C), 1680–1560; ν(C–C), 1480; ν(C–H), 1393; ν(C–O),1250–1060.(Fig. S5) Details of crystallographic parameters are provided in Table S1, S2 and S3.

{[Cd_2(bpe)$_2$(3,3-dmglu)$_2$]}$_n$(1'): The single crystals of **2** were heated to 250°C in a hot air oven. After 3 h, light white crystals of **1'**suitable for X-ray analysis were obtained. Details of crystallographic parameters are provided in Table S1.

Physical Measurements. C, H, and N analyses were performed on a Heraeus CHNS analyzer. Infrared spectra (4000–400 cm^{-1}) were taken on KBr pellet, using PerkinElmer Spectrum BX-II IR spectrometer. Powder X-ray diffraction (PXRD) data were collected on a Bruker D8 Discover instrument with Cu-Kα radiation. Thermo gravimetric analysis (TGA) was carried out on a PerkinElmer STA 8000 thermal analyzer under nitrogen atmosphere with a flow rate of 10 cm^3 min^{-1} at a temperature range of 30–600 °C. UV–Vis spectra were recorded on a Perkin Elmer Lambda 35 UV–Vis spectrophotometer. ^1H NMR spectra were recorded at ambient temperatureon Bruker Avance 300 instrument. The chemical shifts (δ) and coupling constants (J) were expressed in ppm and Hz, respectively.

Sorption Measurements. The adsorption isotherms of N_2 (at 77 K) and CO_2 (at 195 K) for **1** and **2** were measured using QuantachromeAutosorb-iQ adsorption instrument. All operations were computer–controlled and automatic. High purity gases were used for the adsorption measurements (nitrogen, 99.999%; carbon dioxide, 99.95%). At the beginning the as synthesized compounds of **1** and **2** (~90 mg each) were placed in the sample tube and dehydrated at 393 K, under a 1×10^{-1} Pa vacuum for about 4 hrs prior to measurement of the isotherms. Helium gas (99.999% purity) was introduced in the gas chamber and allowed to diffuse into the sample chamber to measure the dead volume. Taking samples of **1** and **2** the N_2 adsorptions were carried out at 77 K maintained by a liquid–nitrogen bath; whereas CO_2 adsorptions were measured at 195 K (temperature maintained by dry ice–acetone cold bath) taking **1** and **2** in the pressure range from 0 to 1 bar. The amount of gas adsorbed were calculated from the pressure difference ($P_{cal} - P_e$), where P_{cal} is the calculated pressure with no gas adsorption and P_e is the observed pressure at equilibrium. The solvent adsorption isotherms for H_2O were measured at 298 K in the pressure region from 0 to 24 torr for H_2O, in their vapour state by taking the compounds of **1** and **2** using the same instrument. All the samples (~90 mg each) were activated under similar conditions as mentioned earlier. The solvent molecule used to generate the vapour, was degassed fully by repeated evacuation. The dead volume was measured with helium gas.

Crystallographic Data Collection and Refinement. The single crystal of compound **1, 2** and **1'** was mounted on a thin glass fiber with commercially available super glue. X-ray single crystal data collection of all the crystals were performed at room temperature using Bruker APEX II diffractometer, equipped with a normal focus, sealed tube X-ray source with graphite monochromated Mo-Kα radiation (λ= 0.71073Å). The data were integrated using SAINT[1]

program and the absorption corrections were made with SADABS.[2] The structure was solved by SHELXS-2016[3] using Patterson method and followed by successive Fourier and difference Fourier synthesis. Full matrix least-squares refinement was performed on F^2 using SHELXL-2016[3] with anisotropic displacement parameters for all non-hydrogen atoms except C23 in **1** and **1'**. During refinement one carbon atom (C23) of 3,3-dmglu moiety is found highly disordered and therefore splited in two part (C23A and C23B) considering 0.5 occupancy of each thereafter refined isotropically imposing a DFIX restrains. The hydrogen atoms, bounded to this methyl carbon are not fixed however it has been added to the total molecular formula for both the compounds. All other hydrogen atoms of **1** were fixed geometrically by HFIX command and placed in ideal positions. The potential solvent accessible area or void spaces were calculated using the PLATON[4] multipurpose crystallographic software. All the calculations were carried out using SHELXS-2016,[3] SHELXL-2016,[3] WinGX system Ver-1.80,[6] and TOPOS.[7] Data collection and structure refinement parameters along with crystallographic data for **1, 2** and **1'** are given in Table S1. The selected bond lengths and angles are given in Table S2 and S3.

Nanoindentation Details: Crystals were mounted using feviquick glue on a stainless-steel round shaped sample holder having smooth surface in such an orientation so that the major faces would be indented. Face indices were identified from SCXRD (Fig. S5) and found that (001) is the major face of both parent and photo-cyclised crystals. The experiment was carried out using a nanoindenter (Hysitron Triboindenter, TI Premier, Minneapolis, USA) with a three-sided pyramidal Berkovich diamond indenter tip of radius 120 nm having an in situ Scanning Probe Microscopy (SPM) facility. Before nanoindentation testing, the tip area function was calculated from a series of indentations on a standard fused quartz sample. The indentations were performed under the load control mode fixing the maximum load constant (P_{max}) at 1000 μN. The rates of loading and unloading were both 200 μN/s with 5 sec duration and a 2 sec holding period was applied at the maximum indentation depth. Almost seven indentations were performed for each crystal and SPM images of the indentation impressions were captured immediately just after unloading to avoid any time dependent elastic shape recovery of the residual impression. The obtained P−h curves were analyzed using the standard Oliver−Pharr method[8] to extract the required parameters; elastic modulus (Ey), and hardness (H) of the crystals.

Structural description along with figures and tables related to crystal structures:

Structure description of compound 1: Compound **1** crystallizes in the monoclinic $P2_1/c$ space group (Z = 4) and the structural analysis reveals the formation of a two-fold interpenetrated 3D pillared-layer framework structure (Fig. 1a). The asymmetric unit of **1** contains two crystallographically independent Cd(II) centers (Cd1 and Cd2), two molecules of 3,3-dmglu ligand and two molecules of bpe linker (Fig. S1). The hepta-coordinated Cd1 with CdO_5N_2 coordination environment shows distorted pentagonal bipyramidal geometry where the equatorial sites are occupied by five oxygen atoms (O1, O2, $O3^a$, $O4^a$ and $O4^b$) from three different 3,3-dmgluligands and two nitrogen atoms (N1 and $N2^c$) from two different bpe linkers occupy the axial positions (Fig. S1). However, the hexa-coordinated Cd2 shows distorted octahedral geometry with CdO_4N_2 coordination environment (Fig. S1). The equatorial positions of Cd2 are occupied by four oxygen atoms (O5, O6, $O7^e$ and $O8^f$) from two different 3,3-dmgluligands and two nitrogen atoms (N3 and N4) from two different bpe linkers occupy the axial positions (Fig. S1). Selected bond lengths and bond angles for **1** are shown in the Tables S2. In case of Cd1, each 3,3-dmgluligand connects the adjacent three Cd(II) centers by bis-chelation and mono oxo-bridging fashion to create wavy type metal-carboxylate 2D (4,4) layer in the crystallographic *bc* plane, where both the metal and respective carboxylate behave as 3-connected nodes (Fig. S2). The linear bpe linkers connect the 2D metal-carboxylate sheet to create a bi-pillared 3D structure (Fig. 1b and Fig. S3) in such a manner that the distance between the centers of the adjacent C=C bonds of bpe are around 4.0 A° (Fig. 1b and Fig. S3). On the other hand, for Cd2, each 3,3-dmglu ligand connects adjacent three Cd(II) centers through bridging bidented and chelating fashion to create almost flat 2D metal-carboxylate (4,4) layer in the crystallographic *bc* plane (Fig. S2). These 2D layers are also connected by linear bpe linkers to form bi-pillared 3D structure in such a manner that the distance between the centers of the adjacent C=C bonds of bpe are around 4.8 A° (Fig. 1c and Fig S3). These two 3D bi-pillared arrangements for both Cd1 and Cd2 are interpenetrated to each other forming two fold interpenetrated 2(1+1) 3D structure (Fig. 1a and Fig S3). The structure of **1** is found to be microporous with total solvent accessible estimated void calculated using PLATON of 127.0 $Å^3$which is 3.4 % of the total crystal volume (3742.6 $Å^3$) (Table S1). The TOPOS[2] analysis

reveals that the structure of **1** can be represented as a (3,5) connected bi-nodal interpenetrating net with point symbol$\{4.6^2\}\{4.6^6.8^3\}$.

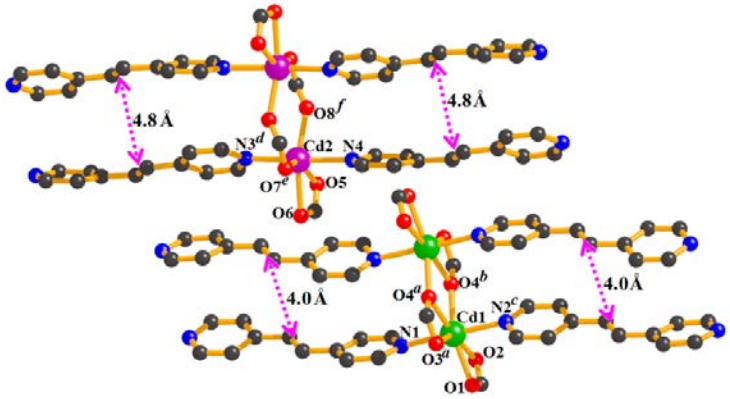

Fig. S1 A perspective view of the coordination environment of Cd1 and Cd2 in **1**. Cd1 (green), Cd2 (Pink), O (red), N (blue) and C (black). The separation of C=C in both the frameworks are depicted by magenta dotted lines.

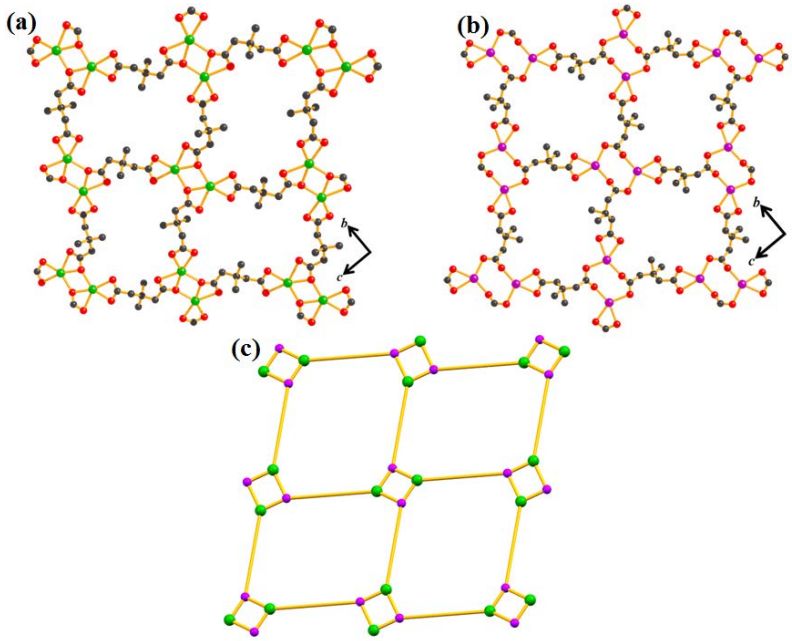

Fig. S2(a) View of wavy type 2D metal-dicarboxylate sheet with hepta-coordinated Cd1 in **1**; (b) view of almost flat 2D metal-dicarboxylate sheet with hexa-coordinated Cd2 in **1**; (c) simplified topological representation of 2D metal-carboxylate (4,4) layer.

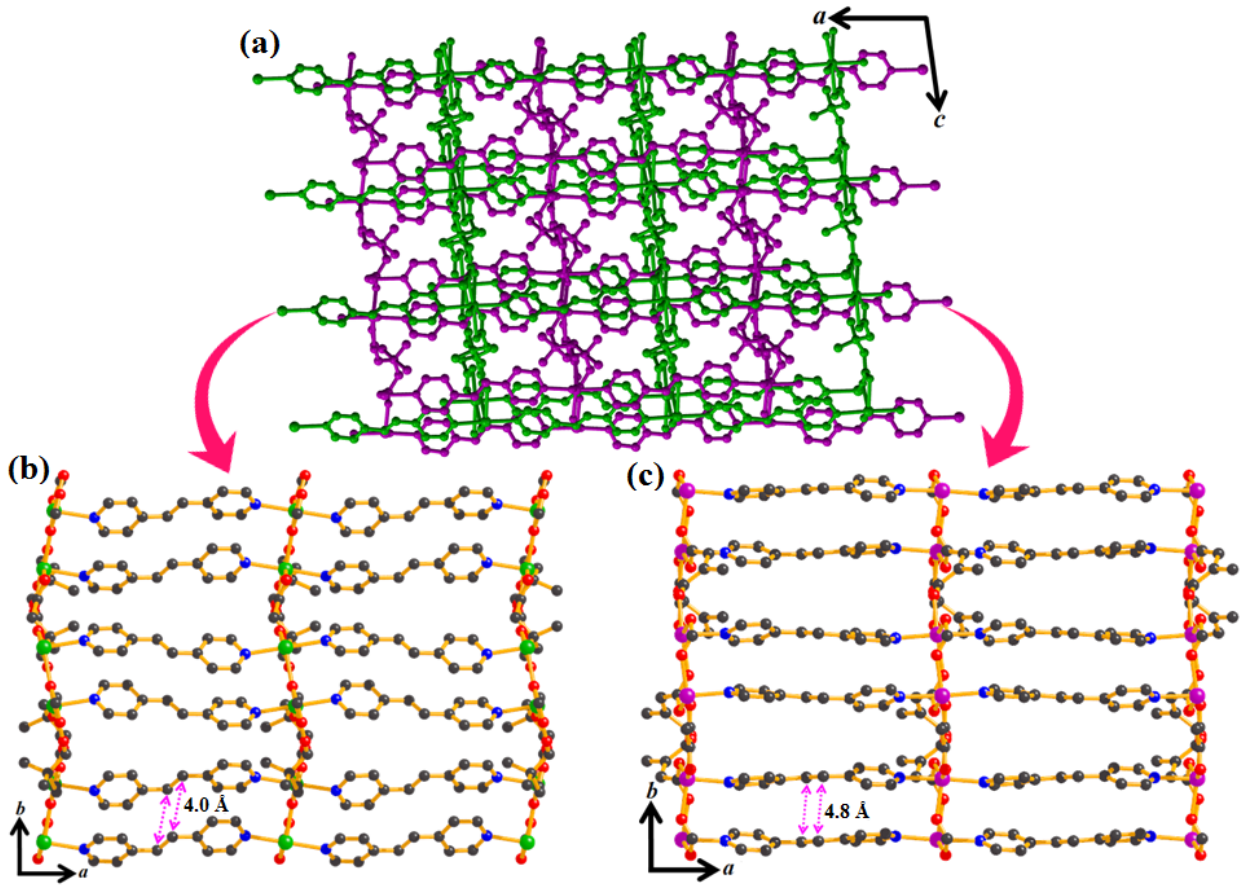

Fig. S3 (a) Overall interpenetrated 3D structure of **1**; (b,c) structural drawing of two 3D nets separately constructed by Cd1 and Cd2 that are part of the overall structure in **1**. The separation of C=C bonds in both the frameworks is depicted by magenta dotted lines.

Structure description of compound 2: Compound **2** crystallizes in the monoclinic *C2* space group (Z = 4) and the structural analysis reveals the formation of a 2-fold interpenetrated 3D framework structure(Fig.1d). The asymmetric unit of **2** also contains two crystallographically independent Cd(II) centers (Cd1 and Cd2), two molecules of 3,3-dmglu ligand and one molecule of rctt-tpcb linker (Fig. S4). The hepta-coordinated Cd1 displays distorted pentagonal bipyramidal geometry with CdO_5N_2 coordination environment where the five oxygen atoms (O1, $O2^d$, O5, $O7^b$ and $O8^b$) of three different 3,3-dmgluligands form the equatorial plane and two nitrogen atoms (N1 and $N2^c$) of two different rctt-tpcb ligands occupy the axial positions (Fig. S4). Whereas, the hexa-coordinated Cd2 shows distorted octahedral geometry with CdO_4N_2 coordination environment (Fig. S4). Four oxygen atoms ($O2^d$, O3, O4 and $O6^d$) from two

different 3,3-dmgluligands comprise the equatorial positions and two nitrogen atoms (N3^{d} and N4^{e}) of two different rctt-tpcb ligands occupy the axial positions (Fig. S4). Selected bond lengths and bond angles for **2** are shown in the Tables S3. Both the Cd(II) centers are connected by three different bridging 3,3-dmglu ligands by means of chelation and oxo-bridging to form 2D metal-carboxylate (4,4) layer in crystallographic *bc* plane (Fig. S5). These sheets are further connected by rctt-tpcb linkers to form pillared 3D network structure with large void space (Fig.1e-f and Fig. S6), which is by two-fold interpenetration (Fig.1d and Fig. S6). The structure of **2** is found to be microporous with total solvent accessible estimated void of 218.0 Å^3 which is 5.9 % of the total crystal volume (3694.4 Å^3). The structure can be described by TOPOS software, as a (3,4,5)-connected tri-nodal two fold interpenetrated net with Schläfli symbol{4.8^2}2{4^2.8^4}{4^6.8^4}2.

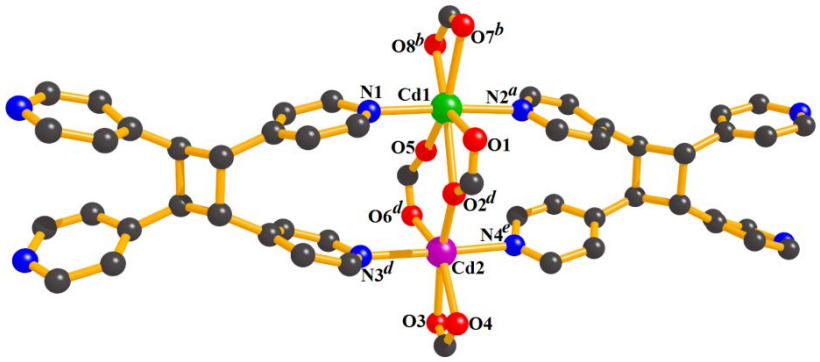

Fig. S4 A perspective view of the coordination environment of Cd1 and Cd2 in **2**. Cd1 (green), Cd2 (Pink), O (red), N (blue) and C (black).

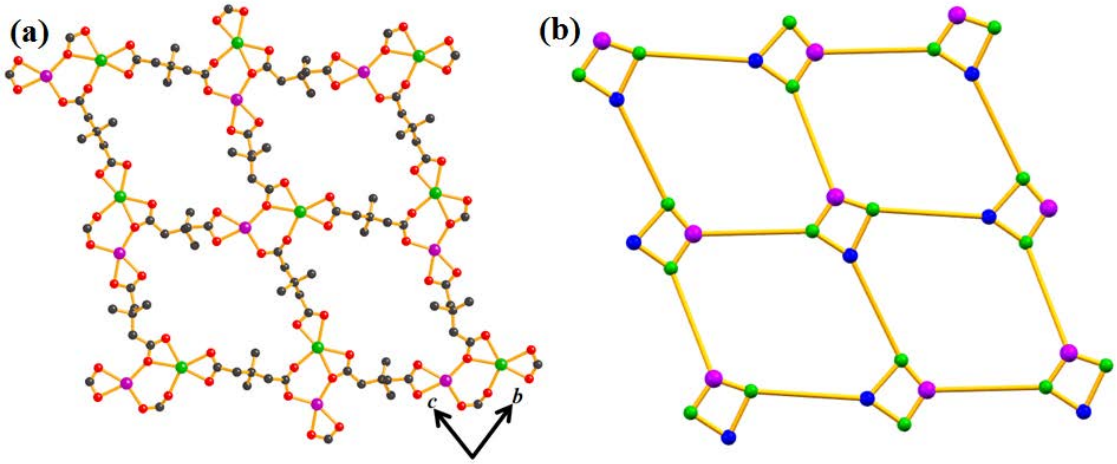

Fig. S5 (a) View of wavy type 2D metal-dicarboxylate sheet in **2**; (b) simplified topological representation of 2D metal-carboxylate (4,4) layer in **2**.

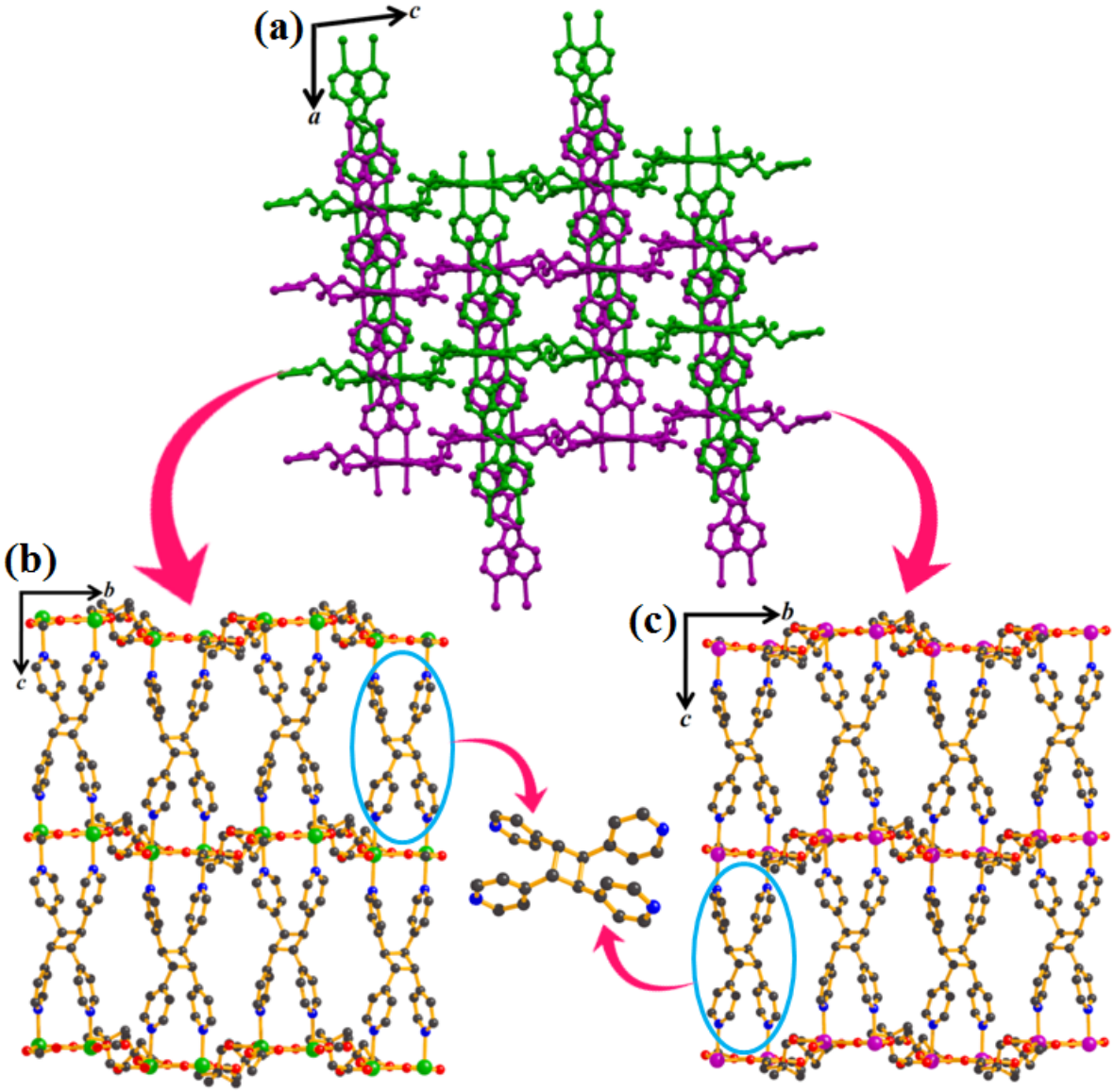

Fig. S6 (d) Overall interpenetrated 3D structure of **2**; and (e,f) structural drawing of two 3D nets separately constructed by Cd1 and Cd2 that are involved in interpenetration to give the overall structure in **2**. Cd1 (green), Cd2 (Pink), O (red), N (blue) and C (black).

Table S1: Crystallographic and structural refinement parameters for complex **1**, **2** and **1'**

	1	**2**	**1'**
formula	$C_{38}H_{40}Cd_2N_4O_8$	$C_{38}H_{40}Cd_2N_4O_8$	$C_{38}H_{40}Cd_2N_4O_8$
formula weight	905.54	905.56	905.54
crystal system	Monoclinic	Monoclinic	Monoclinic
space group	*P21/c*	*C 2*	*P21/c*
a/ Å	13.9823(5)	13.7767(8)	13.9867(5)
b/Å	15.7734(5)	14.4557(8)	15.7579(5)
c/ Å	17.0202(6)	18.5563(11)	17.0260(5)
α/°	90	90	90
β/°	94.432(2)	91.428(4)	94.278(2)
γ/°	90	90	90
V/ Å^3	3742.6(2)	3694.4(4)	3742.1(2)
Z	4	4	4
D_c/ g cm^{-3}	1.602	1.628	1.602
μ /mm^{-1}	1.193	1.208	1.193
F_{000}	1812	1824	1812
θ range/°	1.5, 27.6	2.0, 27.6	1.5, 27.7
reflections collected	70818	28749	57847
unique reflections	8699	8408	8717
reflections $I > 2\sigma(I)$	5848	5849	6574
R_{int}	0.093	0.067	0.038
goodness-of-fit (F^2)	1.04	1.03	1.04
$R1$ ($I > 2\sigma(I)$) [a]	0.0461	0.0711	0.0423
wR_2($I > 2\sigma(I)$) [a]	0.1140	0.1990	0.1059
$\Delta\rho$ min / max /e Å^3	-0.69, 0.82	-1.01, 2.79	-1.12, 1.59

[a] [a]$R_1 = \Sigma \big| |F_o| - |F_c| \big| / \Sigma |F_o|$. [b] $wR_2 = [\Sigma (w (F_o^2 - F_c^2)^2) / \Sigma w (F_o^2)^2]^{½}$

Table S2: Selected bond lengths (å) and bond angles (°) for complex **1**.

Cd1–N2^{c}	2.365(4)	Cd1–O2	2.469(3)
Cd1–O4^{b}	2.329(3)	Cd2–O5	2.407(3)
Cd1– O3^{a}	2.559(3)	Cd2–O6	2.358(3)
Cd1– O4^{a}	2.347(3)	Cd2–N4	2.359(4)
Cd1–N1	2.355(4)	Cd2–N3^{d}	2.311(4)
Cd1– O1	2.287(3)	Cd2–O8^{f}	2.250(5)
Cd2– O7^{e}	2.301(3)	O2–Cd1–O4^{a}	164.22(10)
O2–Cd1–O3^{a}	143.19(10)	O3^{a}–Cd1–N1	92.71(12)
N1–Cd1–N2^{c}	177.72(12)	O4^{b}–Cd1–N2^{c}	89.45(10)
O4^{b}–Cd1–N1	90.27(10)	O4^{a}–Cd1–N2^{c}	93.69(11)
O4^{a}–Cd1–N1	88.38(11)	O4^{b}–Cd1–O4^{a}	72.46(10)
O3^{a}–Cd1–N2^{c}	89.31(12)	O1–Cd1–O4^{b}	145.60(10)
O3^{a}–Cd1–O4^{b}	124.63(10)	O1–Cd1–O4^{a}	141.38(10)
O3^{a}–Cd1–O4^{a}	52.41(10)	O1–Cd1–N1	95.60(13)
O1–Cd1–O3^{a}	88.99(11)	O2–Cd1–N1	88.27(13)
O1–Cd1–O2	54.35(11)	O2–Cd1–O4^{b}	92.14(10)
O1–Cd1–N2^{c}	83.38(13)	O5–Cd2–N4	84.99(11)
O2–Cd1–N2^{c}	89.48(13)	O5–Cd2–O8^{f}	101.2(2)
O5–Cd2–O6	54.85(14)	O6–Cd2–N4	89.92(13)
O5–Cd2–N3^{d}	91.43(11)	O6–Cd2–O8^{f}	155.73(19)
O5–Cd2–O7^{e}	145.67(14)	N3^{d}–Cd2–N4	174.64(12)
O6–Cd2–N3^{d}	91.26(13)	O7^{e}–Cd2–N4	86.77(13)
O6–Cd2–O7^{e}	91.94(11)	O7^{e}–Cd2–N3^{d}	98.41(13)
O8^{f} –Cd2–N4	83.46(13)	O7^{e}–Cd2–O8^{f}	110.88(19)
O8^{f} –Cd2–N3^{d}	93.36(13)		

[a] Symmetry code: *a* = 2-x, 1/2+y, 1/2–z; *b* = x, –1/2–y, –1/2+z;c=1–x, –y,1–z; d =2–x,1–y,1–z;e=1–x, 1/2+y, 1/2–z; f = x, 1/2–y, –1/2+z

Table S3: Selected bond lengths (å) and bond angles (°) for complex **2.**

Cd1–O1	2.447(13)	Cd2–O3	2.336(15)
Cd1–O2	2.525(14)	Cd2–O4	2.369(15)
Cd1–O5	2.310(18)	Cd2–O2^{d}	2.267(13)
Cd1–N1	2.304(12)	Cd2–O6^{d}	2.256(15)
Cd1–N2^{a}	2.327(11)	Cd2–N3^{d}	2.457(13)
Cd1–O7^{b}	2.445(16)	Cd2–N4^{e}	2.353(11)
Cd1–O8^{b}	2.301(13)		
O1–Cd1–O2	51.5(5)	O8^{b}–Cd1–N2^{a}	88.4(5)
O1–Cd1–O5	126.0(6)	O7^{b}–Cd1–O8^{b}	53.9(6)
O1–Cd1–N1	87.2(5)	O3–Cd2–O4	54.5(5)
O1–Cd1–N2^{a}	89.2(5)	O2^{d}–Cd2–O3	159.5(5)
O1–Cd1–O7^{b}	91.2(5)	O3–Cd2–O6^{d}	97.1(6)
O1–Cd1–O8^{b}	145.1(6)	O3–Cd2–N3^{d}	92.9(7)
O2–Cd1–O5	74.5(6)	O3–Cd2–N4^{e}	88.8(6)
O2–Cd1–N1	86.2(5)	O2^{d}–Cd2–O4	105.1(5)
O2–Cd1–N2^{a}	89.7(5)	O4–Cd2–O6^{d}	150.6(6)
O2–Cd1–O7^{b}	142.6(5)	O4–Cd2–N3^{d}	87.4(5)
O2–Cd1–O8^{b}	163.2(6)	O4–Cd2 –N4^{e}	94.4(5)
O5–Cd1–N1	91.5(8)	O2^{d} –Cd2–O6^{d}	103.3(6)
O5–Cd1–N2^{a}	88.7 (7)	O2^{d}–Cd2–N3^{d}	86.6(7)
O5–Cd1–O7^{b}	142.4(6)	O2^{d}–Cd2–N4^{e}	92.2(7)
O5–Cd1–O8^{b}	88.7(7)	O6^{d} –Cd2–N3^{d}	86.7(6)
N1–Cd1–N2^{a}	175.7(5)	O6^{d} –Cd2–N4^{e}	92.2(6)
O7^{b}–Cd1–N1	96.0(7)	N3^{d}–Cd2–N4^{e}	178.1(7)
O8^{b}–Cd1–N1	96.0(5)	Cd1–O2–Cd2^{c}	124.1(6)
O7^{b}–Cd1–N2^{a}	86.4(7)		

[a] Symmetry code :*a*= –1+x, 1+y, z ; *b* = 3/2–x, 3/2+y, 2–z; c=3/2–x,1/2+y,1–z; d = x,1+y,z; e= –1+x, 1+y, z.

FT-IR

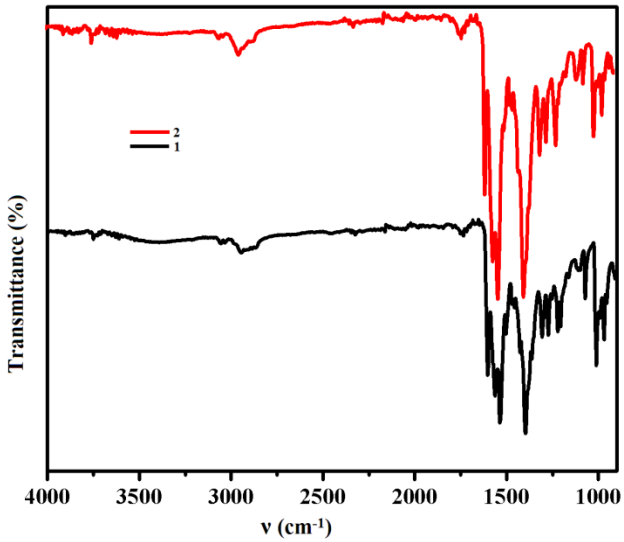

Fig. S7 Combined ATR spectra of **1** and **2**.

PXRD

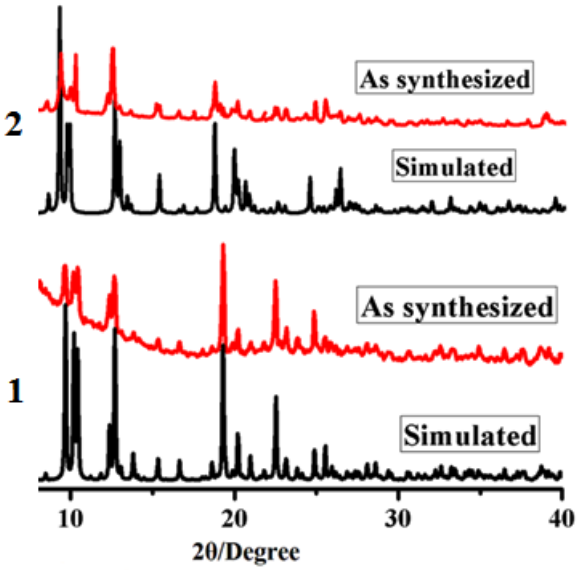

Fig. S8 PXRD pattern of **1** and **2** in different states: (a) simulated (black), (b) as synthesized (red).

NMR Spectra:

To support the SCSC conversion, we have tried to carry out the H^1-NMR spectroscopy of **1** and **2** but the compound found insoluble in all common organic solvent and even in many strong acids. Only it is found soluble in strong HNO_3 and thus the H^1-NMR spectra for **1** and **2** were performed in DMSO-HNO_3. For this, both the compounds were taken in NMR tube and a drop of strong $HNO_3$was added along with DMSO. The mixture was then sonicated for 10 min to dissolve the insoluble MOFs before recording the H^1-NMR spectra. Here aqueous HNO_3 gave an intense peak at δ 4.5-6, whereas the proton signal of the characteristic cyclized cyclobutane rings also come in the same region. As a result, the characteristic peak (of small amount of polymer dissolved in the acid) was submerged and therefore no direct inference could be made from the H^1-NMR regarding the transition. Although the H^1-NMR spectrum of compound **2** and **1**(Fig. S9) was done with few crystals, each characterized by single crystal X-ray diffraction before doing the H^1-NMR in DMSO-HNO_3. The conversion of **1** to **2** is evidenced here partially. Here in the H^1-NMR spectrum of compound **2**, the characteristic peak for the proton of CH=CH went off (which was present in the H^1-NMR spectrum of compound **1**) but the CH proton of the cyclobutane ring is being fully masked in the area of the huge peak of aqueous HNO_3 and could not be analyzed.

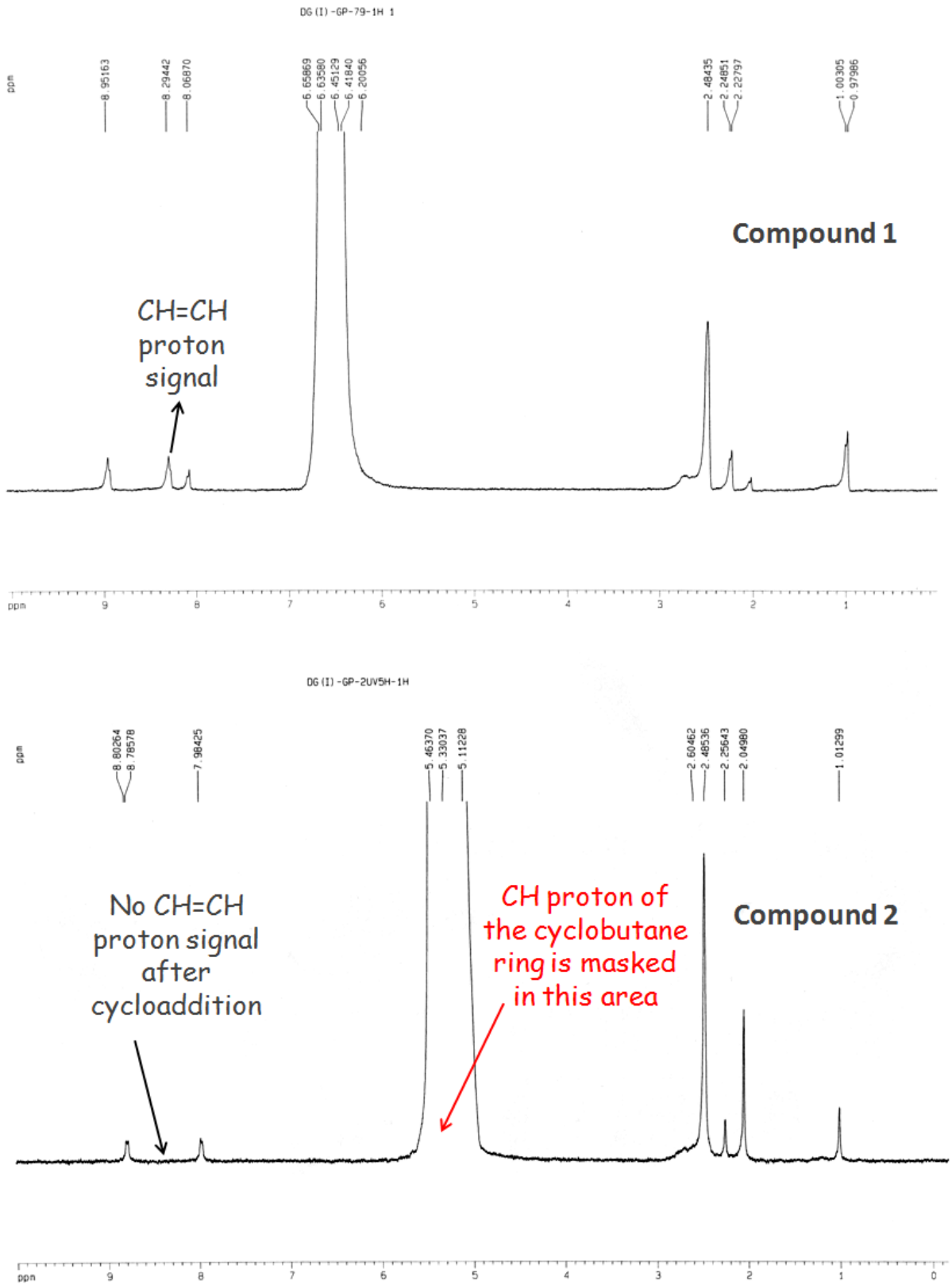

Fig. S9 NMR spectra of **1** and **2**.

TGA

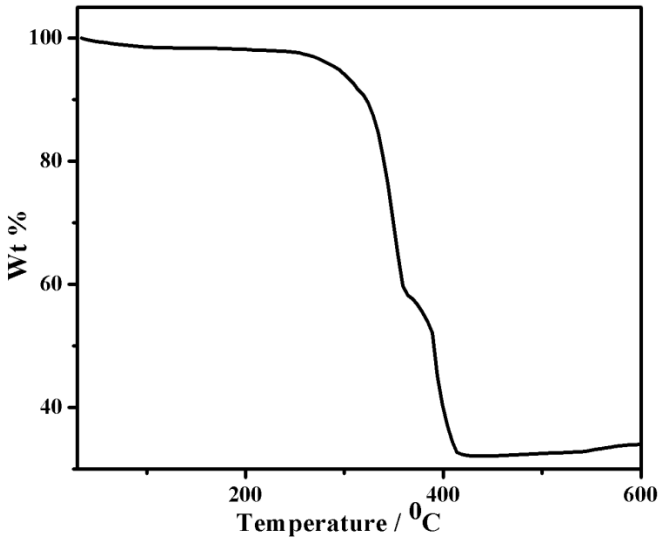

Fig. S10 TGA analysis of **1** at 30 ^{o}C – 600 ^{o}C, showing the stability of the MOF up to 290°C.

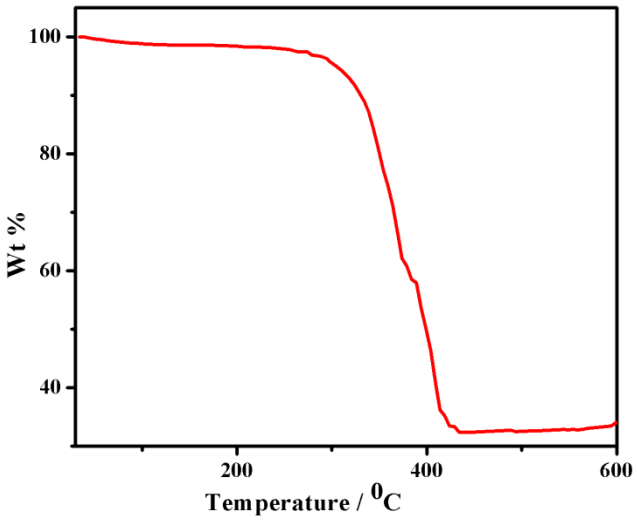

Fig. S11 TGA analysis of **2** at 30 ^{o}C – 600 ^{o}C, showing the stability of the MOF up to 300°C.

Differential Thermal Analyses

Differential Thermal Analyses (DTA) were performed to understand the progress of the cycloaddition reaction. Here compound **1** upon irradiation with UV for 4hours converted to compound **2.** The **2** is also reverting back to **1** upon heating. Therefore, the formation of **2** with UV radiation can be monitored by the reverse thermal transition in the conversion temperature range, in DTA experiment, taking very slow heating rate of 2 degree/minute. In DTA, for the compound **2** (compound **1** on UV exposure for a duration of 4 hours, henceforth represented as **1** @4H UV) significant endothermic peak appear at the temperature range 110°C-210°C with ΔH value ~ 10.4 KJ/mole (Figure SI). This clearly indicates the photo conversion of **1** into **2** that has been reverting back during the DTA study. The same experiment has done with the compound **1** after UV radiation for 1 hour (**1**@1H UV), 2 hours (**1**@2H UV) and 3 hours (**1**@3H UV) (Figure SI). In none of the cases, endothermic curve has been obtained which indirectly proves that there is no conversion from **1** to **2** has been possible, when the UV irradiation has done below 4 hours. From this experiment we have stipulated the UV irradiation time (for the conversion of **1** to **2**) 4 hours and the heating temperature 250°C (for the conversion of **2** to **1**)

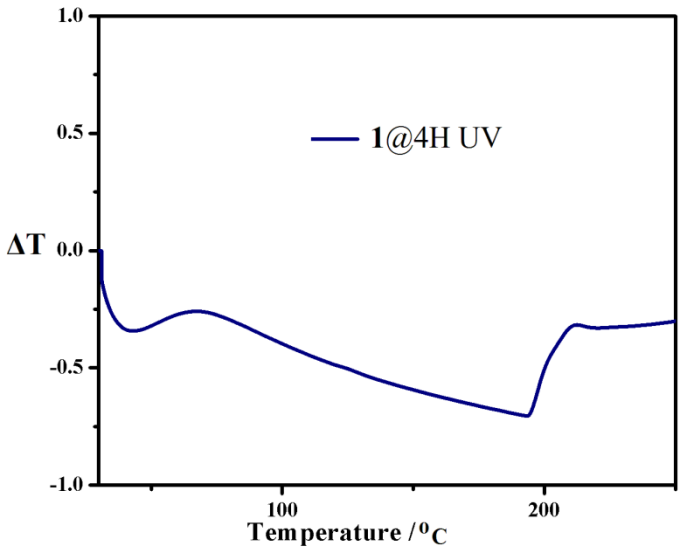

Fig. S12 DTA analysis of **1** @4H UV (**2**) at 30 °C – 250 °C

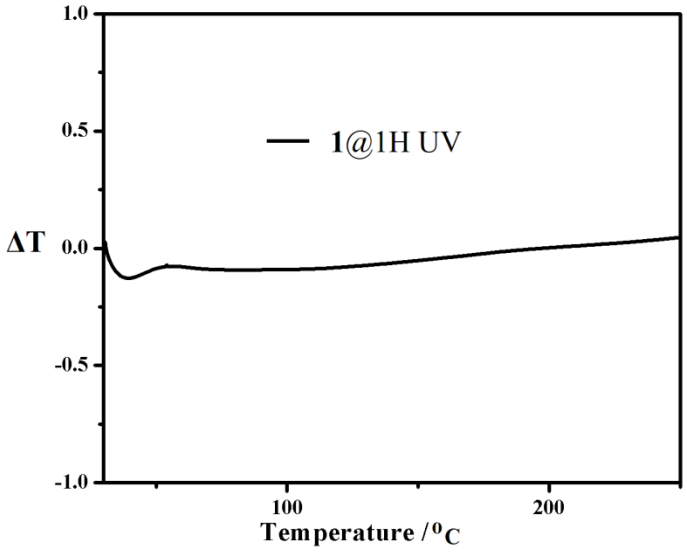

Fig. S13 DTA analysis of **1** @1H UV at 30 ºC – 250 ºC

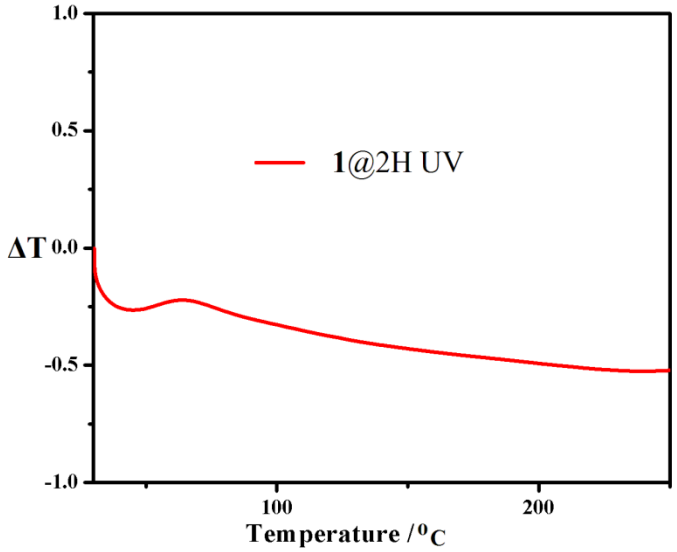

Fig. S14 DTA analysis of **1** @2H UV at 30 ºC – 250ºC

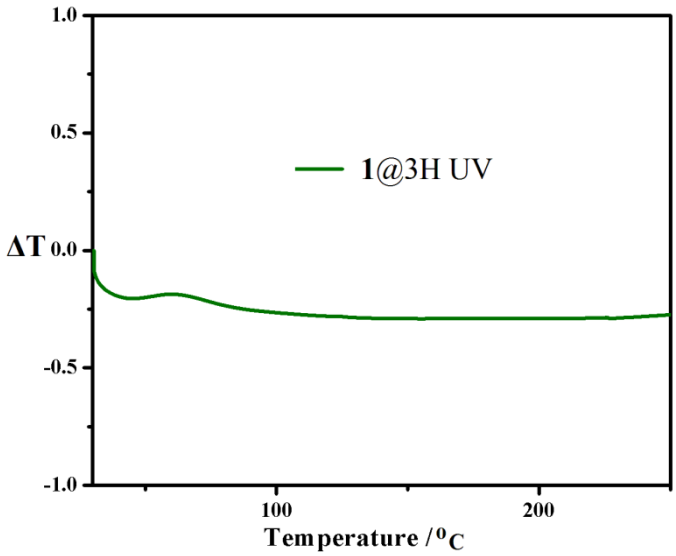

Fig. S15 DTA analysis of **1** @3H UV at 30 ºC – 250 ºC

Face Indexing

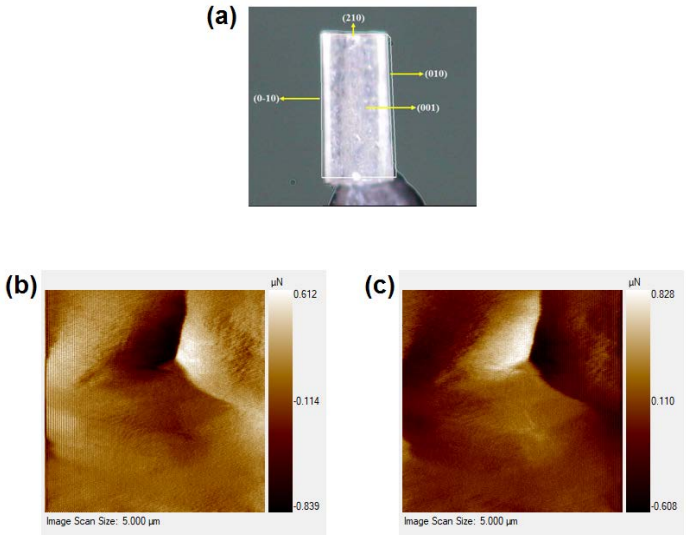

Fig. S16 (a) Face indexed images of real crystal of compound **1**. The SPM images of the residual indent impressions of (b) compound **1**, and (c) compound **2**, respectively.

Table S4: Crystal mechanical properties for compounds **1** and **2**.

Compound	Indented Plane	*H* (GPa) Average	*Ey*(GPa) Average
1	(001)	0.79	6.79
2	(001)	0.87	7.073

Figures Related to Gas and Vapor Sorption

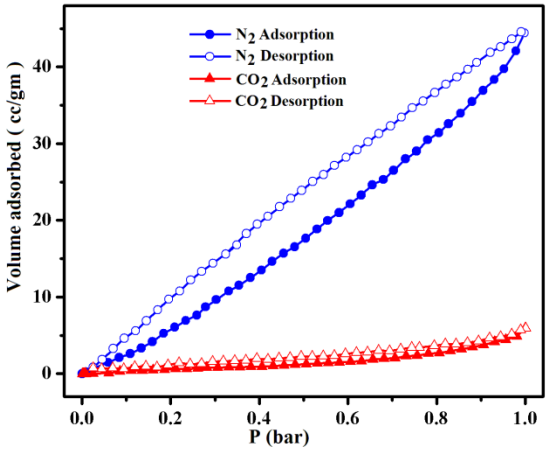

Fig. S17 Different sorption isotherms of **1**; N_2 at 77 K (blue circles), CO_2 at 195 K (red triangles).

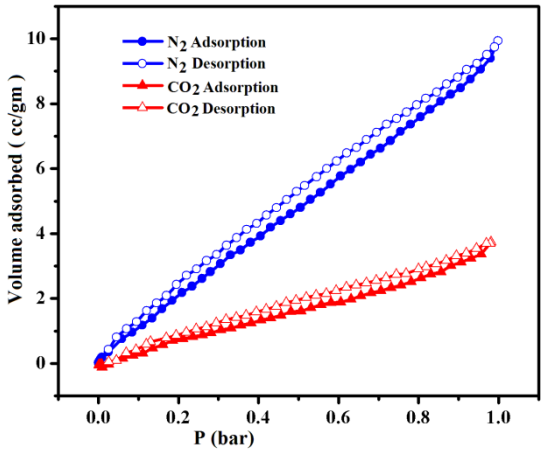

Fig.S18 Different sorption isotherms of **2**; N_2 at 77 K (blue circles), CO_2 at 195 K (red triangles), signifying adsorption (filled) and desorption (empty) curve.

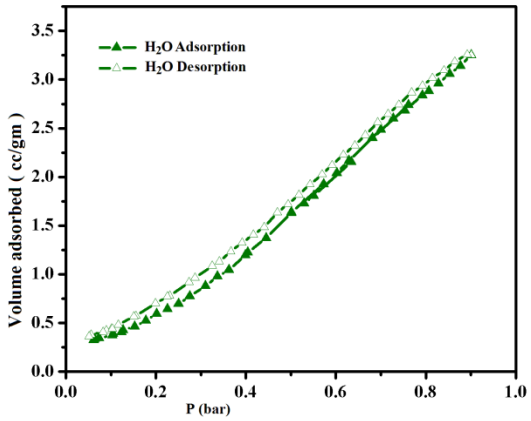

Fig. S19 H_2O sorption (green triangle) of **1** at 298 K; signifying adsorption (filled) and desorption (empty) curve.

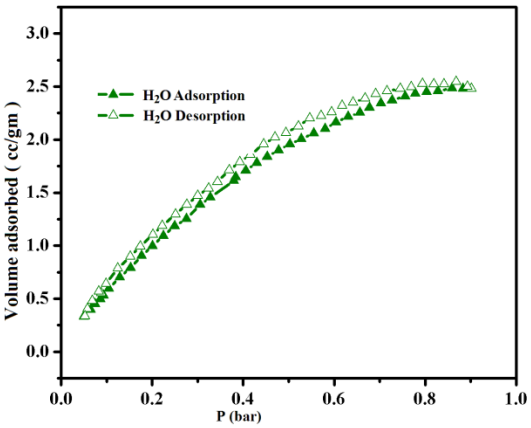

Fig. S20 H_2O sorption (green triangle) of **2** at 298 K; signifying adsorption (filled) and desorption (empty) curve.

UV-VIS

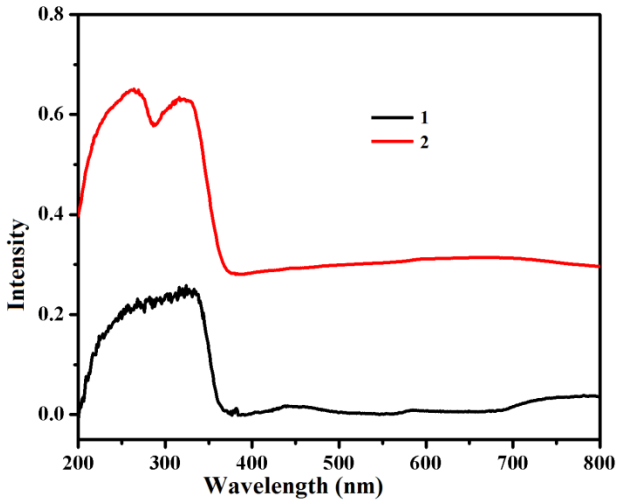

Fig. S20 Combined UV-Vis spectra of **1** and **2**.

References

(1) *SMART (V 5.628), SAINT (V 6.45a), XPREP*, *SHELXTL*, Bruker AXS Inc., Madison, WI, 2004.

(2) Sheldrick, G. M. *SADABS (Version 2.03)*, University of Göttingen, Germany, **2002**.

(3) Sheldrick,G. M. SHELXS-2016, Program for the crystal structure solution, University of Göttingen, Göttingen, Germany, **2016**.

(4) Spek, A. L. *Acta Crystallogr., Sect. D: Biol. Crystallogr.***2009**, *65*, 148.

(5) Farrugia, L. J. *J. Appl. Crystallogr.***1997**, *30*, 565.

(6) Farrugia, L. J. WinGX.*J. Appl. Crystallogr.***1999**, *32*, 837-838.

(7) (a) Blatov, V. A.; Shevchenko, A. P.; Serezhkin, V. N. *J. Appl. Crystallogr.***2000**, *33*, 1193. (b) Blatov, V. A.; Carlucci, L.; Ciani, G.; Proserpio, D. M. *CrystEngComm* **2004**, *6*, 377-395.

(8) W. C. Oliver, M. Pharr, *J. Mater. Res.***1992**, *7*, 1564